NANO LETTERS

pubs.acs.org/NanoLett Letter

Induction and Ferroelectric Switching of Flux Closure Domains in Strained $PbTiO_3$ with Neural Network Quantum Molecular Dynamics

Thomas M. Linker,* Ken-ichi Nomura, Shogo Fukushima, Rajiv K. Kalia, Aravind Krishnamoorthy, Aiichiro Nakano, Kohei Shimamura, Fuyuki Shimojo, and Priya Vashishta

Cite This: *Nano Lett.* 2023, 23, 7456–7462 Read Online

ACCESS | Metrics & More | Article Recommendations | Supporting Information

ABSTRACT: We have developed an extension of the Neural Network Quantum Molecular Dynamics (NNQMD) simulation method to incorporate electric-field dynamics based on Born effective charge (BEC), called NNQMD-BEC. We first validate NNQMD-BEC for the switching mechanisms of archetypal ferroelectric $PbTiO_3$ bulk crystal and 180° domain walls (DWs). NNQMD-BEC simulations correctly describe the nucleation-and-growth mechanism during DW switching. In triaxially strained $PbTiO_3$ with strain conditions commonly seen in many superlattice configurations, we find that flux-closure texture can be induced with application of an electric field perpendicular to the original polarization direction. Upon field reversal, the flux-closure texture switches via a pair of transient vortices as the intermediate state, indicating an energy-efficient switching pathway. Our NNQMD-BEC method provides a theoretical guidance to study electro-mechano effects with existing machine learning force fields using a simple BEC extension, which will be relevant for engineering applications such as field-controlled switching in mechanically strained ferroelectric devices.

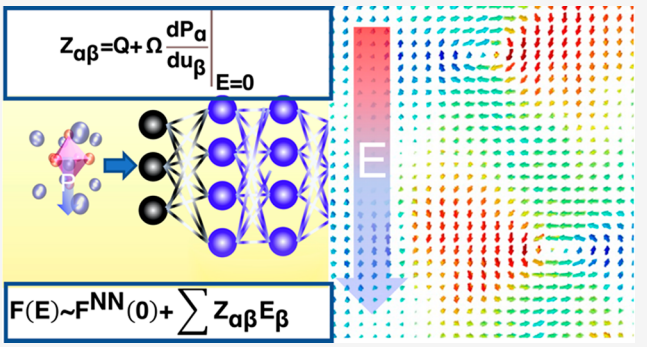

KEYWORDS: *Machine Learning, Molecular Dynamics, Ferroelectric Switching, Polarization Topology*

Over past few years, there has been considerable development in forming topological structures (e.g., skyrmions, merons, vortices, and flux closures) in strained oxide superlattices.[1−6] Dynamical control of these topological structures has garnered great interest for the development of next-generational ferroelectric devices, as they are topologically protected from thermal noise and can be directly manipulated through control of the mechanical strain and polarization boundary conditions that give rise to their emergence. This has created a new field of "ferroelectric topotronics", where one tries to manipulate topological defects through optical, mechanical, or electrical means.[6−12]

Rational design and control of polar topologies require fundamental understanding of their dynamics on picosecond-to-nanosecond time-scales and nano−micrometer length scales.[6] Ab-initio quantum molecular dynamics (MD) simulation is a promising tool to explore the dynamics of emerging topological textures; however, exploring sufficient spatiotemporal scales with required quantum-mechanical (QM) accuracy is computationally intractable. Over the past decade, there has been growing movement to incorporate machine learning (ML) interatomic potentials that offer a comparable accuracy of the underlying QM theory with fractions of the computational cost.[13−15] For example, Linker et al. have developed multiscale NNQMD simulation frameworks to explore optical and mechanical manipulation of various topological structures in $PbTiO_3$ (PTO) based ferroelectric structures.[8,12] However, studying the electric field dynamics with ML interatomic potentials poses a unique challenge, as there is no description of atomic charge in commonly available NNQMD models. Notable breakthrough are so-called the third and fourth generation high-dimensional neural network potentials (HDNNPs) that incorporate some form of charge/coulomb interaction and dynamic charge transfer.[16] However, these methods do not incorporate the rescreening of the electron density from the applied field and require retraining the model parameters in the presence of an electric field.

Here, we propose a simple extension based on the BEC method combined with the existing NNQMD model[8,12] to investigate switching dynamics in an archetypal PTO system. Our NNQMD-BEC scheme naturally takes into account the rescreening effect by the BEC extension to first order. We first

Received: May 22, 2023
Revised: August 5, 2023
Published: August 9, 2023

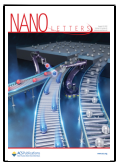

https://doi.org/10.1021/acs.nanolett.3c01885
Nano Lett. 2023, 23, 7456−7462

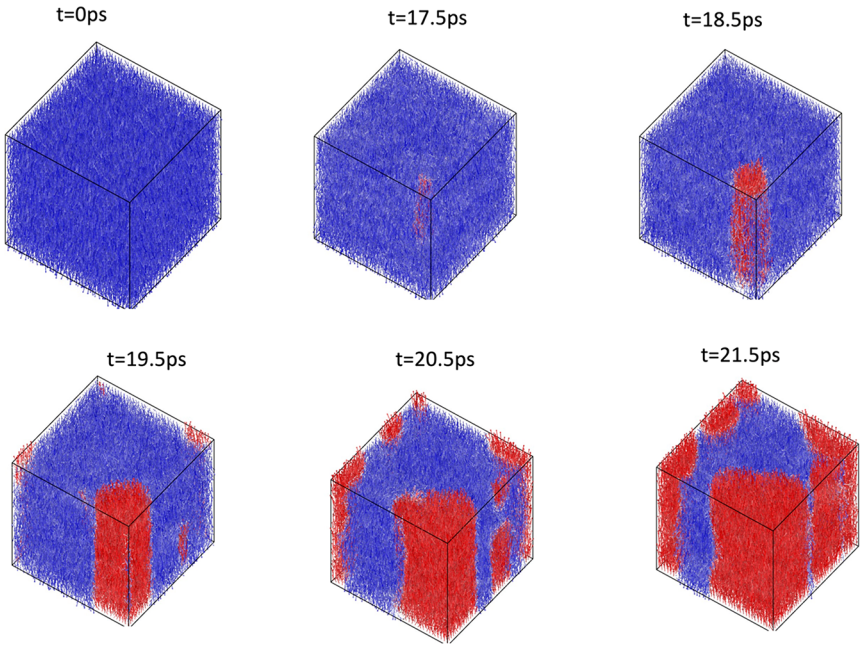

Figure 1. Evolution of polarization in a bulk PTO crystal under an electric field of 3 MV/cm. Red and blue arrows represent the dipole moments that are parallel and antiparallel to the electric field, respectively.

examine the NNQMD-BEC scheme with the well-characterized switching dynamics of bulk PTO crystal and one with 180° DWs. The switching process has been well studied in molecular dynamics simulations with different domain wall geometries.[17,18] In addition, the PTO polarization structure, bonding, and other electronic properties in domain walls, surfaces, and heterostructures have been well studied from first-principles making it an ideal system for validation of the model.[19−21]

After the validation, we examine electric field dynamics of a PTO crystal subjected to a triaxial loading, i.e., biaxial tensile (in the a and b axes) and uniaxial (in the c-axis) compressive loading, to mimic strain conditions often seen in PTO based oxides superlattices and strained thin films.[2,4,5,22,23] We find that, under these strain conditions, an applied electric field perpendicular to the polarization axis can induce a flux closure domain that remains after the removal of the electric field with remnant polarization along the applied field direction. We then finally examine the ferroelectric switching dynamics of the remnant polarization in the flux closure domain, where an efficient energy pathway with a vortex state as the intermediate state is found.

Our NNQMD-BEC scheme utilizes the BEC tensor, which for an atom in a crystal represents the linear response of the electronic polarization of crystal with respect to the displacements from its equilibrium position:[24]

$$Z_{\alpha\beta} = Q + \Omega \frac{\mathrm{d}P_\alpha}{\mathrm{d}u_\beta}\bigg|_{E=0} \qquad (\alpha, \beta \in \{x, y, z\}) \tag{1}$$

where Q is the bare charge, Ω is the unit cell volume, P is the electronic polarization, and u is the displacement of the atom from its equilibrium position.

The same coefficient describes the linear response of atomic force $\vec{F}$ from an applied electric field $\vec{E}$, because both terms are connected to second-order derivative of the energy with respect to atomic displacements and a macroscopic electric field:[24]

$$Z_{\alpha\beta} = \frac{\mathrm{d}F_\alpha}{\mathrm{d}E_\beta} \tag{2}$$

Thus, within a linear response regime, the change in the forces predicted from a neural network model F^α_{NN} may be obtained as

$$F^\alpha_{NN}(E) \sim F^\alpha_{NN}(0) + \sum \frac{\mathrm{d}F_\alpha}{\mathrm{d}E_\beta} E_\beta + O(E^2) \tag{3}$$

assuming F^α_{NN} has learned the ground-truth density functional theory (DFT) forces used to compute the BECs. This will incorporate the change in forces due to not only the electric-field and ionic interactions but also screening and redistribution of electron density due to the high-frequency dielectric constant ϵ_∞.

We examine the dynamics of ferroelectric switching of bulk $PbTiO_3$ utilizing the existing NNQMD force field developed in ref 12. The previously developed NNQMD model was used to predict the ground-state forces, whereas the Born effective charge tensor at the equilibrium $PbTiO_3$ position from the literature[25] was used to apply the electric field. The NNQMD force field in this work utilizes a feed-forward neural network with two hidden layers and 20 nodes in each layer and hyperbolic tangent activation function. To capture local atomic environments, it employs an energy model based on the symmetric functions proposed by Behler and Parrinello.[13,14] The training data consists of multiple density tetragonalities and high temperature configurations and is available at https://zenodo.org/record/7293180. The model is trained in the Aenet software[15] and implemented in the RXMD molecular dynamics software.[26] Complete description of the training process is provided in ref 12. The used NNQMD model was previously validated using various elastic and structural properties[12] and also examined the dynamics of 180°

https://doi.org/10.1021/acs.nanolett.3c01885
Nano Lett. 2023, 23, 7456−7462

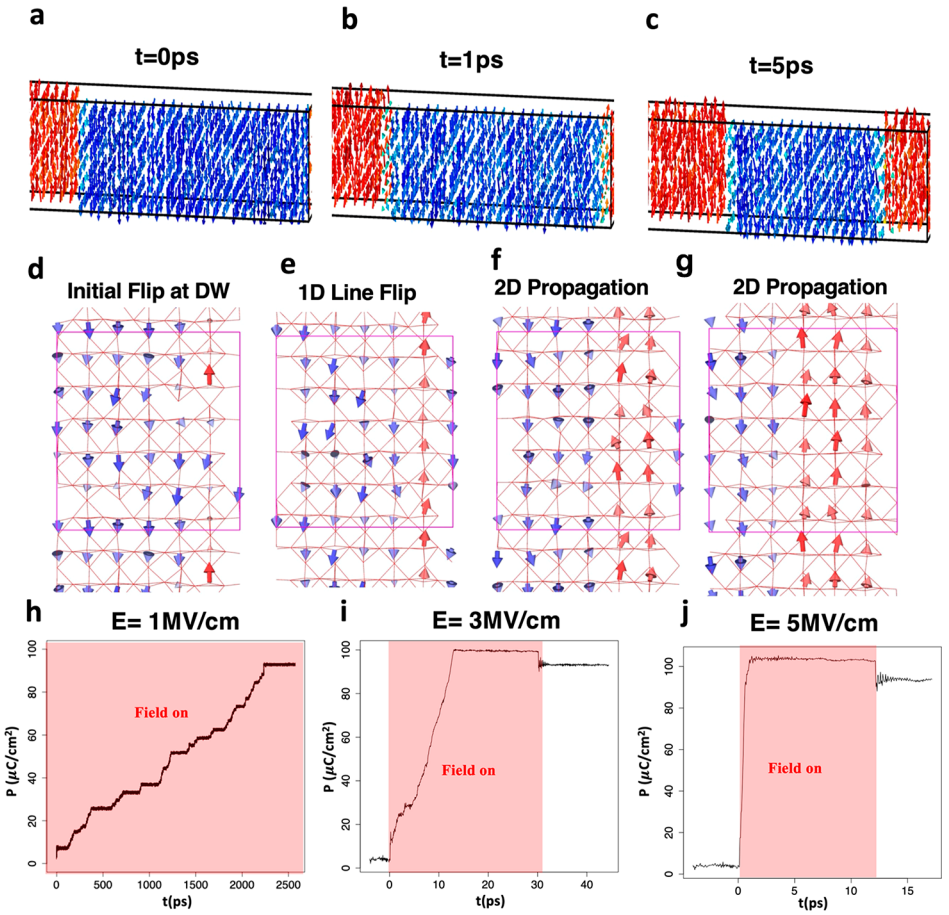

Figure 2. Switching dynamics in a 180° DW at 300 K. (a) Initial DW structure. (b and c) Evolution of DW switching at t = 1 and 5 ps after turning on the electric field, respectively. (d−g) Progression of dipole moment in PTO unit cells at the DW. An initial flip of dipole moment due to the applied electric field quickly grows into a line of polarizations parallel to the field (1D growth), followed by the lateral growth (2D growth) at the DW. (h−j) the time evolution of total polarization with three different field strengths.

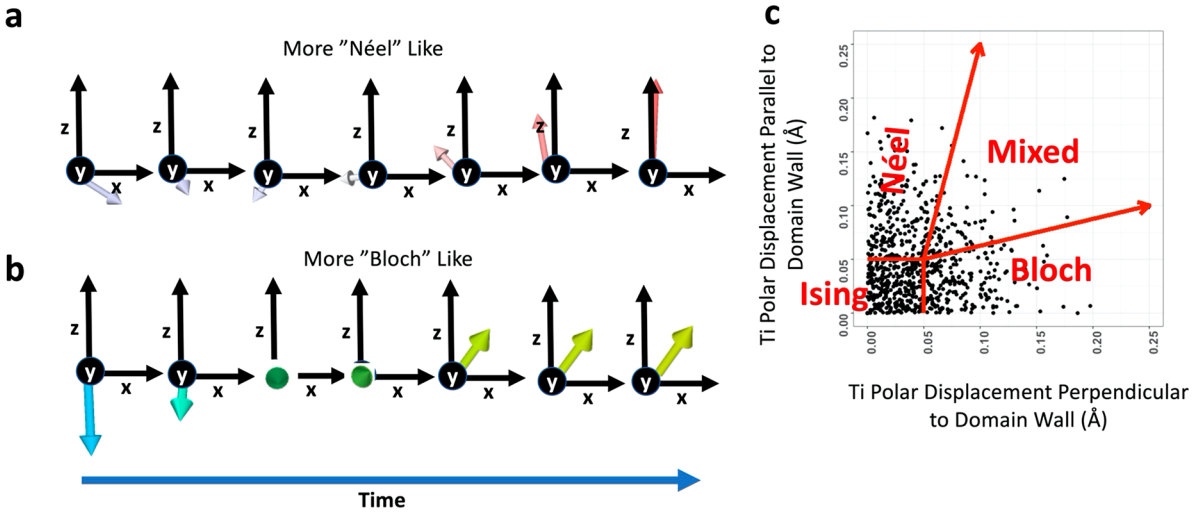

Figure 3. Polarization rotation during switching. Panel (a) shows dynamics during the switching process for a given unit cell that resembles the Néel-type rotation, while panel (b) shows more Bloch-type rotation. The DW wall is along the x axis, and the polarization axis is the z axis in this figure. Each snapshot is 50 fs apart. (c) Distribution of Ti polar displacements right at the point of switching (D_z = 0 Å).

DWs and polar skyrmion domains that has shown consistent behavior with state-of-the-art experimental imaging techniques and phase-field simulation studies.[3,27] The system consists of 40 × 40 × 40 PTO unit cells with uniform polarization along the negative c-axis at the beginning of the simulation. The PTO crystal was subjected to an electric field of 3 MV/cm in the opposite direction of the system polarization, i.e., along the positive c-axis. The polarization dynamics with snapshots at several time points are listed in Figure 1. The first nucleation of opposite polarization domain was observed after 17.5 ps, and

https://doi.org/10.1021/acs.nanolett.3c01885
Nano Lett. 2023, 23, 7456−7462

in the following picosecond (18.5 ps from field activation) a columnar domain has formed via a series of dipole moment reversal events. Subsequently the columnar domain grew laterally showing the 2D propagation outward from its DW. The nucleation-and-growth behavior is found similar to previous MD simulation studies of ferroelectric switching in PTO crystals.[17,18]

To obtain atomistic-level insights of the switching dynamics, we have created a PTO crystal consisting of 50 × 6 × 6 unit cells with two 180° DWs inserted at the middle and the edge of the system. The system is thermalized at 300 K and then subjected to an electric field of 3 MV/cm along the polarization direction (*c*-axis). Figure 2a shows the thermalized DW before applying an electric field. The dipole moments at the DW are rather diffuse with reduced magnitude, which is consistent with previous molecular dynamics study.[17,18] Figure 2b,c shows the evolution of the DW under the field. The switching of polarization started at the DW and steadily progressed through the system. In the DW, a few dipole moments flipped initially due to thermal fluctuation and field bias (Figure 2d), which subsequently cascaded into dipoles along the *c* axis (Figure 2e). The line of flipped dipole moments further influenced the adjacent dipole moments and laterally propagated within the DW (Figure 2f,g). We examined the switching dynamics with three different field strengths (Figure 2h−j). With the lowest field strength of 1 MV/cm, the DW switching was completed in 2.2 ns, showing a discrete stick−slip behavior.

During the switching process, we also monitor the dynamics of dipole moments measured by the displacement of the Ti atom relative to the oxygen octahedron, in which the center of the octahedron is taken as the reference position (i.e., $\boldsymbol{P} = 0$). Figure 3a,b shows the time evolution of individual dipole moments during the switching process under an electric field of 3 MV/cm. The *x* axis is along the DW direction, and the *z* axis is the polarization axis. The dynamics in Figure 3a closely resembles that of a Néel-type rotation around the polarization axis, while in Figure 3b the dynamics resemble those of a Bloch-type rotation. We further investigated the switching dynamics by categorizing the individual dipole moments as Bloch-, Néel-, or Ising-type rotation based on the distribution of dipole moment orientation at the middle point of the switching (see Figure 2c). Though the classification of rotation types (Bloch, Néel, and Ising) can be improved by further sampling, the significant presence of Bloch and Néel components shown in Figure 3c indicates the importance of non-Ising switching pathways inside DWs. This indicates that at room temperature ferroelectric switching is truly a multiphonon process as the typical transverse optical modes responsible for the ferroelectricity displace the atoms only in an Ising-like manner. Such knowledge will be relevant for comparing to ultrafast switching pathways in the optical or terahertz (THz) regime which is induced by coupling to these modes directly.

We next examined the electro-mechano effect in polarization dynamics by using a triaxially strained PTO lattice (compressed in the polarization direction and expanded in the other two directions) that are often seen in the ferroelectric−dielectric superlattices.[2,4,5,22,23] We have applied a triaxial strain of 2% compression along the *c*-axis and 2% expansion along the *a*- and *b*-axes. We first thermalized and strained a 32 × 32 × 4 supercell structure at temperature 300 K over 30 ps, then applied an electric field of 3 MV/cm. Figure 4a presents the

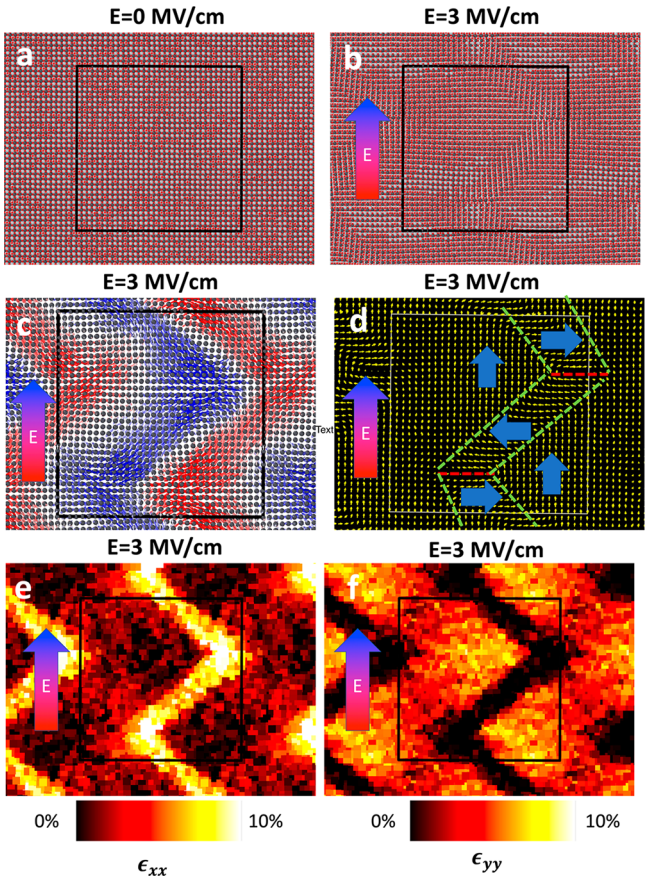

Figure 4. Polarization dynamics in strained PTO under an electric field. (a) *a*−*b* plane lattice structure of PTO prior to application of the electric field. (b) Plastically deformed *a*−*b* plane after application of the electric field. (c) Displacement of Pb atoms under the electric field. Polarization texture exhibits a Bloch-like rotation in response to the applied field. (d−f) Polarization and strain fields (ϵ_{xx} and ϵ_{yy}) under the electric field, respectively.

initial strained PTO structure thermalized at 300 K before applying the electric field, in which the system shows a uniform distribution of atoms without any *a*−*b* polarization texture. Through the triaxial strain, the polarization along the original *c* axis is reduced and polarization becomes more favorable to be induced along the *a* and *b* axes. We found that applying an electric field along the *a* axis induces a net polarization on the system along the field direction, while zero polarization along the other directions and a resulting flux closure texture. Figure 4b illustrates the atomic coordinates in the *a*−*b* plane, which has deformed from the applied field configuration in Figure 4a. The displacement of lead (Pb) atoms from the zero-field configuration is illustrated in Figure 4c, and dipole moments on the *a*−*b* plane are illustrated in Figure 4d. The polarization texture results from a Bloch-type rotation's atomic planes from the zero-field structure. The texture forms due to the complex interplay between the applied electric field and the induced strains. Through compressing along *c* and expanding along the *a*−*b* directions, we have lowered the energy barrier to polarize in the system in the *a*−*b* plane. Thus, applying a field to uniformly polarize the system along either the *a* or *b* axis will drive the system to expand along the field direction. Since the system is still constrained, this causes the atomic planes to slip and form high regions of local strain to compensate for the system's inability to expand, which is illustrated in Figure 4e,f.

https://doi.org/10.1021/acs.nanolett.3c01885
Nano Lett. 2023, 23, 7456−7462

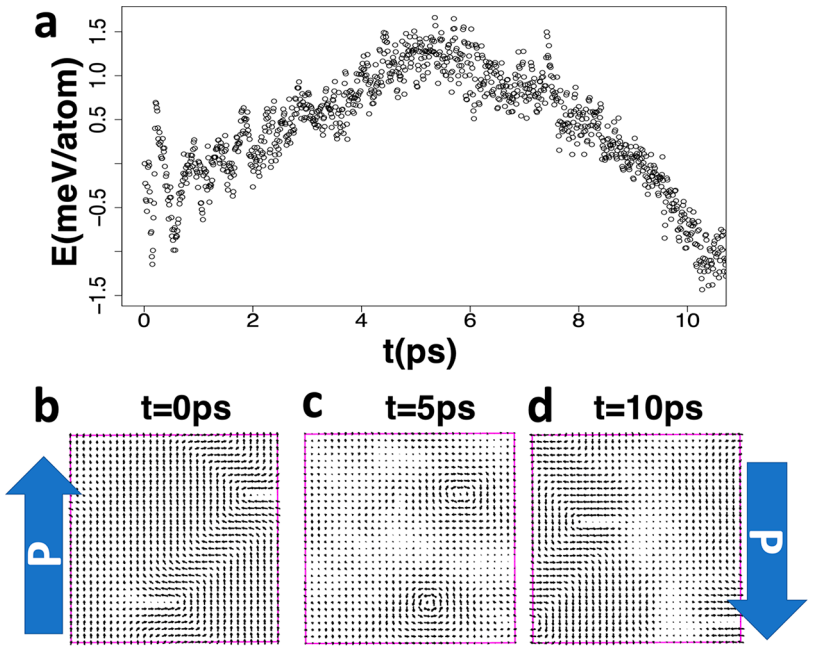

Figure 5. Dynamical switching of flux closure domain subjected an electric field of 300 kV/cm. (a) Potential energy profile (including the field energy) during the switching process. (b−d) Evolution of dipole field during the electric field reversal. A pair of vortices has emerged in the middle and facilitated the switching.

The behavior is similar to the buckling of atomic planes observed in the ferroelectric and chirality switching of polar vortices in strained $SrTiO_3$(STO)/PTO superlattices.[9] Here, we further report that our buckling dynamics have a topological character in the form of Bloch rotation of the atoms. The emergence of such a topology from competition between strain and electrical stimuli has yet to be discussed in the literature. Of note, while the unit-cells undergo Bloch rotations, this is not the polarization topology that emerges. This is because the unit-cell rotations are a result of the long-range strain constraints and the polarization emerges from small local displacements within the unit-cells that cause the Ti and Pb atoms to be off center. Understanding the link between these two different topologies will be critical for developing energy efficient topotronic devices. The induced texture and net polarization remained unchanged after removal of the electric field, indicating a potentially ferroelectric state. The dynamics after removal of the field are illustrated in Supplementary Movie S1.

In dielectric/ferroelectric superlattices, local polarization curl in the form of vortices and flux closure domains forms due to both charge and strain boundary conditions applied on the ferroelectric layer;[3] however, topological structures have formed in strained PTO thin films from strain and surface interaction alone.[4] Our results demonstrate how introduction of an external field can plastically deform the lattice, introducing topological defects that are maintained by strain boundary conditions alone after removal of the field. Such dynamics are likely relevant to electrical manipulations of strained PTO thin films, such as polar Meron lattices in strained PTO.[4]

We next examined the switching dynamics of the flux-closure state by applying an electric field against the induced polarization, (i.e., changing the field direction) to see if the flux closure state could be ferroelectrically switched. We found that the net polarization can be switched. By monitoring the potential energy of the system during the switching process, we observed a clean double-well energy structure in which the initial and the final states are separated by a well-defined energy barrier. This energy barrier is illustrated in Figure 5a. Figure 5b−d displays the polarization patterns at the initial state (time t = 0 ps), during the transition (t = 5 ps), and after the switching (t = 10 ps), respectively. It was found that a field of 300 kV/cm was required to cleanly switch the structure within 10 ps. This field was much smaller than was required in the bulk and DW systems to obtain a similar switching speed. During the switching, we found the formation of a pair of vortices with opposite chirality (i.e., clockwise and counter-clockwise) near the kinks of the flux closure structure (Figure 5c). Each vortex with the radius of roughly 3 nm has zero net polarization. By going through the vortex pair texture with zero net polarization, switching of the flux closure texture may be facilitated without incurring polarization perpendicular to the applied electric field, thereby realizing an energy efficient switching pathway. A video of the dynamical switching is shown in Supplementary Movie S2.

In conclusion, we have developed a NNQMD-BEC method to explore the electro-mechano response of switching dynamics in PTO. Our NNQMED-BEC scheme has successfully reproduced a conventional layer-by-layer growth mechanism during 180° DW switching. During the DW switching however we found a mixed Bloch- and Néel-type character in dipole moments rotations that is also found in the DW structure of PTO at low temperature.[25] This indicates that at room temperature ferroelectric switching is truly a multiphonon process and will be of interest when comparing the optical or THz switching of ferroelectricity which are typically aimed at coupling to optical ferroelectric modes that displace the atoms in an Ising-like manner. We then examined the electric field response of a triaxially strained PTO lattice where the flux closure texture can be permanently induced, even after turning the electric field off. Flux closure domains

https://doi.org/10.1021/acs.nanolett.3c01885
Nano Lett. 2023, 23, 7456−7462

have technological interest due to their potential for high-density nonvolatile ferroelectric random access memory applications, as well as novel sensor and transducer applications.[1] We find that the flux closure emerges from buckling dynamics that have topological character in the form of Bloch rotation of the atoms. This is not the polarization topology that emerges, which we ascribe to the unit-cell rotations being a result of the long-range strain constraints, and the polarization emerges from small local displacements within the unit-cells that causes the Ti and Pb atoms to be off center.

We then examined the electric field response of a triaxially strained PTO lattice where the flux closure texture can be permanently induced even after turning the electric field off. Our simulation has also revealed an energy-efficient switching pathway going through the formation of a transient vortex pair while keeping the lateral net polarization as zero.

The NNQMD-BEC method described in this work offers a simple but effective drop-in theoretical tool for many existing ML force fields to study the electro-mechano dynamics. Understanding such dynamics will be relevant in electrical manipulations in novel ferroelectric devices involving nano-structured superlattice and standalone thin films.[6]

■ ASSOCIATED CONTENT

Supporting Information

The Supporting Information is available free of charge at https://pubs.acs.org/doi/10.1021/acs.nanolett.3c01885.

Video of dynamics after removal of the field in creation of the flux closure domain; vectors are colored by polarization along the direction the field was originally applied (*b* axis) (MP4)

Video of dynamics during switching of the flux closure domain; vectors are colored by polarization along the *b* axis (MP4)

■ AUTHOR INFORMATION

Corresponding Author

Thomas M. Linker − *Collaboratory for Advanced Computing and Simulations, University of Southern California, Los Angeles, California 90089-0242, United States; Stanford PULSE Institute, SLAC National Accelerator Laboratory, Menlo Park, California 94025, United States;* orcid.org/0000-0002-0504-4876; Email: tlinker@stanford.edu

Authors

Ken-ichi Nomura − *Collaboratory for Advanced Computing and Simulations, University of Southern California, Los Angeles, California 90089-0242, United States*

Shogo Fukushima − *Department of Physics, Kumamoto University, Kumamoto 860-8555, Japan*

Rajiv K. Kalia − *Collaboratory for Advanced Computing and Simulations, University of Southern California, Los Angeles, California 90089-0242, United States*

Aravind Krishnamoorthy − *Collaboratory for Advanced Computing and Simulations, University of Southern California, Los Angeles, California 90089-0242, United States;* orcid.org/0000-0001-6778-2471

Aiichiro Nakano − *Collaboratory for Advanced Computing and Simulations, University of Southern California, Los Angeles, California 90089-0242, United States;* orcid.org/0000-0003-3228-3896

Kohei Shimamura − *Department of Physics, Kumamoto University, Kumamoto 860-8555, Japan*

Fuyuki Shimojo − *Department of Physics, Kumamoto University, Kumamoto 860-8555, Japan*

Priya Vashishta − *Collaboratory for Advanced Computing and Simulations, University of Southern California, Los Angeles, California 90089-0242, United States;* orcid.org/0000-0003-4683-429X

Complete contact information is available at: https://pubs.acs.org/10.1021/acs.nanolett.3c01885

Author Contributions

T.L., K.N., R.K., A.K., A.N., K.S., F.S., and P.V. designed the work and NNQMD framework. T.L. designed the NNQMD-BEC scheme. T.L. and K.N. trained the original NNQMD model. T.L. performed the NNQMD simulations. T.L. wrote the first draft of the manuscript. All participated in the analysis of the data and writing the manuscript

Notes

The authors declare no competing financial interest.

■ ACKNOWLEDGMENTS

This work was supported as part of the Computational Materials Sciences Program funded by the U.S. Department of Energy, Office of Science, Basic Energy Sciences, under Award Number DE-SC0014607. Simulations were performed at the Argonne Leadership Computing Facility under the DOE INCITE and Aurora Early Science programs and at the Center for Advanced Research Computing of the University of Southern California.

■ REFERENCES

(1) Tang, Y. L.; Zhu, Y. L.; Ma, X. L.; Borisevich, A. Y.; Morozovska, A. N.; Eliseev, E. A.; Wang, W. Y.; Wang, Y. J.; Xu, Y. B.; Zhang, Z. D.; Pennycook, S. J. Observation of a Periodic Array of Flux-Closure Quadrants in Strained Ferroelectric $PbTiO_3$ Films. *Science.* **2015**, *348* (6234), 547−551.

(2) Yadav, A. K.; Nelson, C. T.; Hsu, S. L.; Hong, Z.; Clarkson, J. D.; Schlepuëtz, C. M.; Damodaran, A. R.; Shafer, P.; Arenholz, E.; Dedon, L. R.; Chen, D.; Vishwanath, A.; Minor, A. M.; Chen, L. Q.; Scott, J. F.; Martin, L. W.; Ramesh, R. Observation of Polar Vortices in Oxide Superlattices. *Nature* **2016**, *530* (7589), 198−201.

(3) Das, S.; Tang, Y. L.; Hong, Z.; Gonçalves, M. A. P.; McCarter, M. R.; Klewe, C.; Nguyen, K. X.; Gómez-Ortiz, F.; Shafer, P.; Arenholz, E.; Stoica, V. A.; Hsu, S. L.; Wang, B.; Ophus, C.; Liu, J. F.; Nelson, C. T.; Saremi, S.; Prasad, B.; Mei, A. B.; Schlom, D. G.; Íñiguez, J.; García-Fernández, P.; Muller, D. A.; Chen, L. Q.; Junquera, J.; Martin, L. W.; Ramesh, R. Observation of Room-Temperature Polar Skyrmions. *Nature* **2019**, *568* (7752), 368−372.

(4) Wang, Y. J.; Feng, Y. P.; Zhu, Y. L.; Tang, Y. L.; Yang, L. X.; Zou, M. J.; Geng, W. R.; Han, M. J.; Guo, X. W.; Wu, B.; Ma, X. L. Polar Meron Lattice in Strained Oxide Ferroelectrics. *Nat. Mater.* **2020**, *19*, 881.

(5) Hsu, S.-L.; McCarter, M. R.; Dai, C.; Hong, Z.; Chen, L.-Q.; Nelson, C. T.; Martin, L. W.; Ramesh, R. Emergence of the Vortex State in Confined Ferroelectric Heterostructures. *Adv. Mater.* **2019**, *31* (36), No. 1901014.

(6) Tian, G.; Yang, W. D.; Gao, X. S.; Liu, J.-M. Emerging Phenomena from Exotic Ferroelectric Topological States. *APL Mater.* **2021**, *9* (2), 20907.

(7) Du, K.; Zhang, M.; Dai, C.; Zhou, Z. N.; Xie, Y. W.; Ren, Z. H.; Tian, H.; Chen, L. Q.; Van Tendeloo, G.; Zhang, Z. Manipulating Topological Transformations of Polar Structures through Real-Time Observation of the Dynamic Polarization Evolution. *Nat. Commun.* **2019**, *10* (1), 4864.

(8) Linker, T.; Nomura, K.; Aditya, A.; Fukshima, S.; Kalia, R.; Krishnamoorthy, A.; Nakano, A.; Rajak, P.; Shimmura, K.; Shimojo, F.; Vashishta, P. Exploring Far-from-Equilibrium Ultrafast Polarization Control in Ferroelectric Oxides with Excited-State Neural Network Quantum Molecular Dynamics. *Sci. Adv.* **2022**, *8*, eabk2625.
(9) Behera, P.; May, M. A.; Gomez-Ortiz, F.; Susarla, S.; Das, S.; Nelson, C. T.; Caretta, L.; Hsu, S.-L.; McCarter, M. R.; Savitzky, B. H.; Barnard, E. S.; Raja, A.; Hong, Z.; Garcia-Fernandez, P.; Lovesey, S. W.; van der Laan, G.; Ercius, P.; Ophus, C.; Martin, L. W.; Junquera, J.; Raschke, M. B.; Ramesh, R. Electric Field Control of Chirality. *Sci. Adv.* **2022**, *8* (1), No. eabj8030.
(10) Stoica, V. A.; Laanait, N.; Dai, C.; Hong, Z.; Yuan, Y.; Zhang, Z.; Lei, S.; McCarter, M. R.; Yadav, A.; Damodaran, A. R.; Das, S.; Stone, G. A.; Karapetrova, J.; Walko, D. A.; Zhang, X.; Martin, L. W.; Ramesh, R.; Chen, L. Q.; Wen, H.; Gopalan, V.; Freeland, J. W. Optical Creation of a Supercrystal with Three-Dimensional Nanoscale Periodicity. *Nat. Mater.* **2019**, *18* (4), 377−383.
(11) Das, S.; Hong, Z.; Stoica, V. A.; Gonçalves, M. A. P.; Shao, Y. T.; Parsonnet, E.; Marksz, E. J.; Saremi, S.; McCarter, M. R.; Reynoso, A.; Long, C. J.; Hagerstrom, A. M.; Meyers, D.; Ravi, V.; Prasad, B.; Zhou, H.; Zhang, Z.; Wen, H.; Gómez-Ortiz, F.; García-Fernández, P.; Bokor, J.; Íñiguez, J.; Freeland, J. W.; Orloff, N. D.; Junquera, J.; Chen, L. Q.; Salahuddin, S.; Muller, D. A.; Martin, L. W.; Ramesh, R. Local Negative Permittivity and Topological Phase Transition in Polar Skyrmions. *Nat. Mater.* **2021**, *20* (2), 194−201.
(12) Linker, T.; Nomura, K.; Fukushima, S.; Kalia, R. K.; Krishnamoorthy, A.; Nakano, A.; Shimamura, K.; Shimojo, F.; Vashishta, P. Squishing Skyrmions: Symmetry-Guided Dynamic Transformation of Polar Topologies Under Compression. *J. Phys. Chem. Lett.* **2022**, *13* (48), 11335−11345.
(13) Behler, J.; Parrinello, M. Generalized Neural-Network Representation of High-Dimensional Potential-Energy Surfaces. *Phys. Rev. Lett.* **2007**, *98* (14), No. 146401.
(14) Behler, J. Perspective: Machine Learning Potentials for Atomistic Simulations. *J. Chem. Phys.* **2016**, *145* (17), 170901.
(15) Artrith, N.; Urban, A. An Implementation of Artificial Neural-Network Potentials for Atomistic Materials Simulations: Performance for TiO2. *Comput. Mater. Sci.* **2016**, *114*, 135−150.
(16) Behler, J. Four Generations of High-Dimensional Neural Network Potentials. *Chem. Rev.* **2021**, *121* (16), 10037−10072.
(17) Shin, Y.-H.; Grinberg, I.; Chen, I.-W.; Rappe, A. M. Nucleation and Growth Mechanism of Ferroelectric Domain-Wall Motion. *Nature* **2007**, *449* (7164), 881−884.
(18) Liu, S.; Grinberg, I.; Rappe, A. M. Intrinsic Ferroelectric Switching from First Principles. *Nature* **2016**, *534* (7607), 360−363.
(19) Meyer, B.; Vanderbilt, D. Ab Initio Study of Ferroelectric Domain Walls in $PbTiO_3$. *Phys. Rev. B* **2002**, *65* (10), No. 104111.
(20) Eglitis, R. I.; Vanderbilt, D. Ab Initio Calculations of $BaTiO_3$ and $PbTiO_3$ (001) and (011) Surface Structures. *Phys. Rev. B* **2007**, *76* (15), No. 155439.
(21) Eglitis, R. I.; Bocharov, D.; Piskunov, S.; Jia, R. Review of First Principles Simulations of STO/BTO, STO/PTO, and SZO/PZO (001) Heterostructures. *Crystals.* **2023**, *13* (5), 799.
(22) Kim, K.-E.; Jeong, S.; Chu, K.; Lee, J. H.; Kim, G.-Y.; Xue, F.; Koo, T. Y.; Chen, L.-Q.; Choi, S.-Y.; Ramesh, R.; Yang, C.-H. Configurable Topological Textures in Strain Graded Ferroelectric Nanoplates. *Nat. Commun.* **2018**, *9* (1), 403.
(23) Han, L.; Addiego, C.; Prokhorenko, S.; Wang, M.; Fu, H.; Nahas, Y.; Yan, X.; Cai, S.; Wei, T.; Fang, Y.; Liu, H.; Ji, D.; Guo, W.; Gu, Z.; Yang, Y.; Wang, P.; Bellaiche, L.; Chen, Y.; Wu, D.; Nie, Y.; Pan, X. High-Density Switchable Skyrmion-like Polar Nanodomains Integrated on Silicon. *Nature* **2022**, *603* (7899), 63−67.
(24) Gonze, X.; Lee, C. Dynamical Matrices, Born Effective Charges, Dielectric Permittivity Tensors, and Interatomic Force Constants from Density-Functional Perturbation Theory. *Phys. Rev. B* **1997**, *55* (16), 10355−10368.
(25) Behera, R. K.; Lee, C.-W.; Lee, D.; Morozovska, A. N.; Sinnott, S. B.; Asthagiri, A.; Gopalan, V.; Phillpot, S. R. Structure and Energetics of 180 Domain Walls in PbTiO3 by Density Functional Theory. *J. Phys.: Condens. Matter* **2011**, *23* (17), 175902.
(26) Nomura, K.; Kalia, R. K.; Nakano, A.; Rajak, P.; Vashishta, P. RXMD: A Scalable Reactive Molecular Dynamics Simulator for Optimized Time-to-Solution. *SoftwareX* **2020**, *11*, No. 100389.
(27) Pereira Gonçalves, M. A.; Escorihuela-Sayalero, C.; Garca-Fernández, P.; Junquera, J.; Íñiguez, J. Theoretical Guidelines to Create and Tune Electric Skyrmion Bubbles. *Sci. Adv.* **2019**, *5* (2), No. eaau7023.

https://doi.org/10.1021/acs.nanolett.3c01885
Nano Lett. 2023, 23, 7456−7462